CERN-SPSC-2024-018 / SPSC-SR-349
29/04/2024

NP06/ENUBET annual report 2024 for the SPSC

The ENUBET Collaboration

F. Acerbi[a,b], I. Angelis[x], L. Bomben[e,p], M. Bonesini[e], F. Bramati[e,f], A. Branca[e,f], C. Brizzolari[e,f], G. Brunetti[f], M. Calviani[r], S. Capelli[e,p], S. Carturan[d,g], M.G. Catanesi[h], S. Cecchini[i], N. Charitonidis[r], F. Cindolo[i], G. Cogo[d], G. Collazuol[c,d], F. Dal Corso[c], C. Delogu[c,d], G. De Rosa[j,k], A. Falcone[e,f], B. Goddard[r], A. Gola[a], F. Guffanti[e,f], L. Halić[m], F. Iacob[c,d], M.A. Jebramcik[r], C. Jollet[l], V. Kain[r], A. Kallitsopoulou[w], B. Kliček[m], Y. Kudenko[n,u,v], Ch. Lampoudis[x], M. Laveder[c,d], P. Legou[w], A. Longhin[c,d], L. Ludovici[o], E. Lutsenko[e,p], L. Magaletti[h,q], G. Mandrioli[i], S. Marangoni[e,f], A. Margotti[i], V. Mascagna[y,z], N. Mauri[i], J. McElwee[l], L. Meazza[e,f], A. Meregaglia[l], M. Mezzetto[c], M. Nessi[r], A. Paoloni[t], M. Pari[c,d,r], T. Papaevangelou[w], E.G. Parozzi[e,f,r], L. Pasqualini[i,s], G. Paternoster[a], L. Patrizii[i], M. Pozzato[i], M. Prest[e,p], F. Pupilli[c,d], E. Radicioni[h], A.C. Ruggeri[j,k], G. Saibene[e,p], D. Sampsonidis[x], C. Scian[c,d], G. Sirri[i], M. Stipčević[m], M. Tenti[i], F. Terranova[e,f], M. Torti[e,f,1], S. E. Tzamarias[x], E. Vallazza[e], F.M. Velotti[r], and L. Votano[t]

[a]Fondazione Bruno Kessler (FBK), Via Sommarive 18 - 38123 Povo (TN), IT
[b]INFN-TIFPA, Università di Trento, Via Sommarive 14 - 38123 Povo (TN), IT
[c]INFN Sezione di Padova, via Marzolo 8 - 35131 Padova, IT
[d]Università di Padova, via Marzolo 8 - 35131 Padova, IT
[e]INFN Sezione di Milano-Bicocca, Piazza della Scienza 3 - 20133 Milano, IT
[f]Università di Milano-Bicocca, Piazza della Scienza 3 - 20133 Milano, IT
[g]INFN, Laboratori Nazionali di Legnaro, Viale dell'Università 2 - 35020 Legnaro (PD), IT
[h]INFN Sezione di Bari, Via Giovanni Amendola 173 - 70126 Bari, IT
[i]INFN Sezione di Bologna, viale Berti-Pichat 6/2 - 40127 Bologna, IT
[j]INFN, Sezione di Napoli, Strada Comunale Cinthia - 80126 Napoli, IT
[k]Università "Federico II" di Napoli, Corso Umberto I 40 - 80138 Napoli, IT
[l]LP2I Bordeaux, Universitè de Bordeaux, CNRS/IN2P3, 33175 Gradignan, FR
[m]Center of Excellence for Advanced Materials and Sensing Devices, Ruder Boskovic Institute, HR-10000 Zagreb, HR
[n] Institute for Nuclear Research of the Russian Academy of Sciences, 117312 Moscow, RU

[o]INFN Sezione di Roma 1, Piazzale A. Moro 2, 00185 Rome, IT
[p]Università degli Studi dell'Insubria, Via Valleggio 11 - 22100 Como, IT
[q]Università degli Studi di Bari, Via Giovanni Amendola 173 - 70126 Bari, IT
[r]CERN, Esplanade des particules - 1211 Genève 23, CH
[s]Università degli Studi di Bologna, viale Berti-Pichat 6/2 - 40127 Bologna, IT
[t]INFN, Laboratori Nazionali di Frascati, via Fermi 40 - 00044 Frascati (Rome), Italy
[u]National Research Nuclear University "MEPhI", 115409 Moscow, Russia
[v]Moscow Institute of Physics and Technology, 141701 Moscow region, Russia
[w]CEA, Centre de Saclay, Irfu/SPP, F-91191 Gif-sur-Yvette, FR.
[x]Aristotle University of Thessaloniki. Thessaloniki 541 24, GR.
[y]DII, Università degli Studi di Brescia, via Branze 38, Brescia, IT.
[z]INFN, Sezione di Pavia, via Bassi 6, Pavia, IT.

28 April 2024

Contents

1 Introduction

The year 2023 has been significant for NP06/ENUBET, as the Collaboration has successfully published the first complete simulation of the monitored neutrino beamline (see Fig. 1). This accomplishment marks the achievement of the project's primary objectives. In Section 2, we will provide a summary of the key findings from this publication [1]. Furthermore, the ENUBET Demonstrator was finished in 2023 and exposed to the T9 charged-particle beam. While the analysis is still ongoing, we can already state that the detector response has been fully satisfactory and meets the requirements outlined in previous simulations of the beamline. The construction, testing, and analysis of the Demonstrator data are reported in Section 3.

NP06/ENUBET is close to completion. The remaining tasks comprise the publication of the full assessment of systematics and the validation of the instrumented hadron dump. These tasks are currently in progress and will be finished by 2025 (see Secs. 2 and 5).

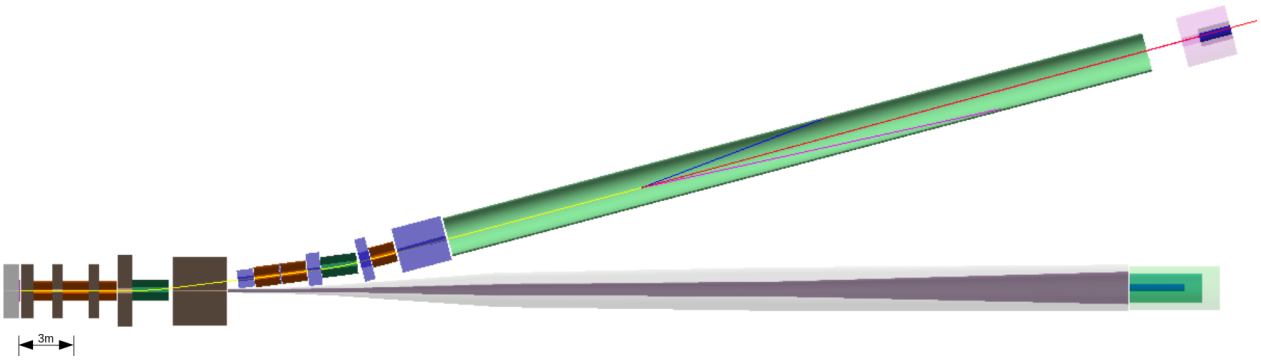

Figure 1: The ENUBET beamline as implemented in G4Beamline, GEANT4 and FLUKA. Primary protons impinge on the target (not shown) located on the left of the figure; secondaries are sign and momentum selected by the transfer line and transported at the entrance of the instrumented decay tunnel (light green). From left to right: the quadrupole triplet (orange) and copper collimators (brown), double-bend momentum selector section composed of two dipoles (green), two quadrupoles, and one momentum copper collimator (brown), and the last quadrupole surrounded by two Inermet180 collimators (blue). The light-green cylinder represents the instrumented decay tunnel where a K_{e3} decay is shown; the red track corresponds to the ν_e traveling towards the neutrino detector. The hadron dump that stops all particles but neutrinos is located at the tunnel exit. Non-interacting protons and forward particles travel inside the proton pipe (in gray) and are stopped by the proton dump (dark green). The neutrino detector considered in ENUBET (mass: 500 tons - not shown in the figure) is located 50 m far from the decay tunnel exit.

The successful NP06 R&D project has led the Collaboration to partner with Physics Beyond Collider (PBC) in order to assess the potential of implementing a CERN project based on the ProtoDUNEs and WTCE [2, 3] as neutrino detectors. This CERN project combines the expertise of NP06 with the advantages offered by the NuTAG tracking technique [4]. In 2023, these groups

formed a joint initiative called Short Baseline Neutrinos at Physics Beyond Collider (SBN@PBC). One of the key accomplishments of SBN@PBC is the development of a beamline that expands the capabilities of [1] in the HyperKamiokande region of interest and significantly reduces the proton requirements of ENUBET. This reduction makes it feasible for CERN to simultaneously operate a monitored neutrino beam alongside SHiP. A summary of these findings can be found in Sec. 4.

2 The ENUBET beamline

2.1 Target optimization

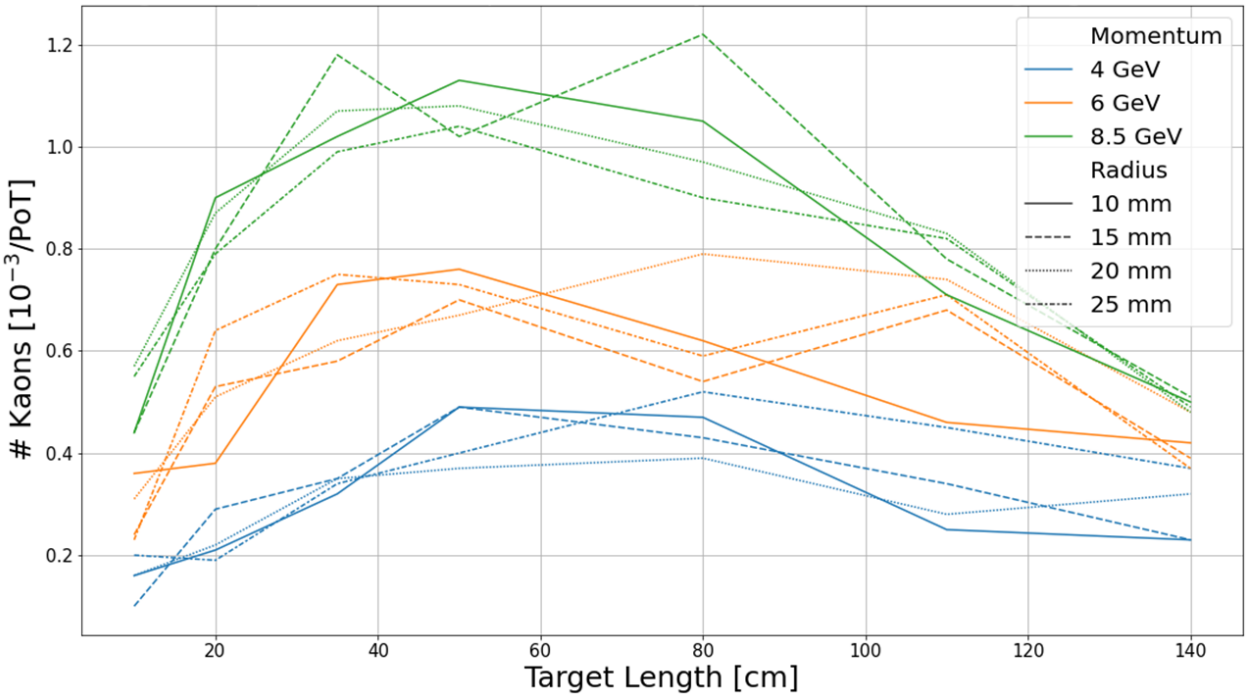

Figure 2: Kaon yields as a function of the graphite target length for a 400 GeV/c proton beam. The figure of merit for the optimization is the number of kaons (10% momentum bite) entering an ideal beamline with ±20 mrad angular acceptance in both planes placed 30 cm after the target. Colors refer to different kaon's momenta while the line style identifies the target radius. The error bars (not plotted to ease the reading) are dominated by the FLUKA interaction modeling systematics and amounts to $\sim 20\%$.

The ENUBET beamline is based on the CERN SPS proton accelerator running at 400 GeV. Simulations were carried out assuming a 2s extraction over a solid-state target. Simulation studies have proven that both for the nominal slow extraction and the burst-mode scheme (e.g. with 10 ms

bursts repeated at 10 Hz) studied in the past, the maximum particle rate in any calorimeter module of the ENUBET decay tunnel remains well below a few hundred of kHz/cm^2, allowing ENUBET to perform lepton monitoring with moderate pile-up effects. The target optimization for ENUBET was performed using the FLUKA [5, 6] and G4beamline [7] Monte-Carlo simulation codes and was carried out assuming the CERN SPS as a proton driver. Even if this beamline can be implemented in any proton driver with an energy of around 100 GeV, the choice of the CERN SPS is particularly attractive when the mean secondary momentum corresponds to 8.5 GeV/c because the number of pions produced per proton hitting the target scales roughly with the energy of the primary protons [8] and the secondary yield at 8.5 GeV/c is close to maximum [9]. Optimization was carried out against a change of dimensions (radius and length of the cylindrical target) and material (graphite, beryllium, Inconel-718). Material comparison has shown a clear advantage of graphite over other materials even in kaon-enriched beams, which confirms expectations since graphite is the material of choice for high-power pion enriched beams. Inconel shows slightly fewer kaon yields than graphite and, given the limited operational experience with this material for high-intensity neutrino beams, has not been investigated any further. Fig. 2 summarizes the kaon yields for different graphite target configurations. The figure of merit (FOM) for the optimization is the number of kaons (10% momentum bite) that enters an ideal beamline with ±20 mrad angular acceptance in both planes placed 30 cm after the target.

2.2 Transfer line and static focusing system

The design of an effective, purely static beamline has been a breakthrough in the ENUBET R&D because it allows for very low pile-up levels, removes the operational complexity of a magnetic horn, and turned out to be highly cost-effective. The fact that the ENUBET signal comes from kaon decays also puts a tight constraint on the beamline length, which has to be short enough to minimize kaon decays before the entrance of the decay tunnel. Hence, the length of the transfer line plays a pivotal role in the optimization process. Even with a transfer line as short as 20 m, about 30% of kaons are lost, and the K/π abundance ratio drops by $\sim$ 25% The beamline optics was optimized using TRANSPORT with a momentum bite of 5%[1]. The best configuration achieved in this optics optimization phase consists of a quadrupole triplet followed by a bending dipole, a pair of quadrupoles, another bending dipole identical to the first one, and a final quadrupole (see Fig. 3). The two dipoles are based on existing CERN magnets that can be operated up to 1.8 T with a field length of 2.038 m and an aperture of 300 mm. Each dipole provides a bending angle of 7.4°, for a total bending of the beam with respect to the primary proton line of 14.8°. Fields at poles in the quadrupoles are kept below 11 kG, for an aperture radius of 15 cm.

Once the beam optics is designed, the full beamline has been implemented and simulated into particle tracking and interaction codes: FLUKA, GEANT4, and G4beamline [10], with the addition of absorbers and collimators between elements, a Tungsten foil after the target to screen positrons that would otherwise reach the instrumented decat tunnel (tagger) and contribute to the

[1]Note that the actual momentum bite of ENUBET after the implementation of tertiary interactions with G4Beamline is 10%.

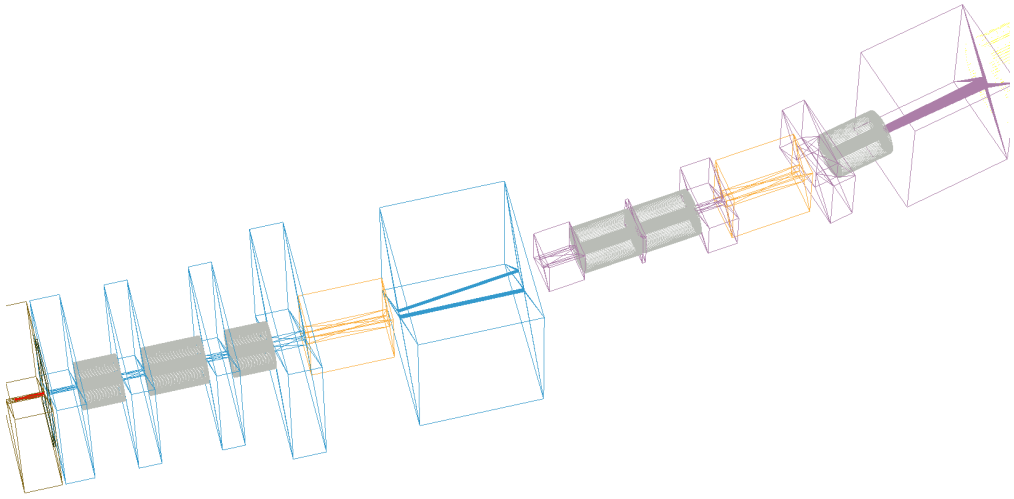

Figure 3: Details of the beamline: in blue the copper collimators, in purple the Inermet180 collimators. Quadrupoles and dipoles are shown respectively in gray and orange. The target (red cylinder) is surrounded by concrete shielding.

background, a low power hadron dump at the end of the decay tunnel and the proton dump. The FLUKA code was instrumental in the simulation of the meson yields after the target and to evaluate the doses at the beamline elements and the instrumentation. The beamline collimation has been designed using copper blocks for the first quadrupole triplet and the momentum collimator, while in the second half of the beamline, the collimators are made of Inermet180, a heavier Tungsten-based alloy employed for the LHC collimators [11]. The collimator design is a multi-parameter problem that can only be solved with intensive numerical simulations. For this reason, NP06/ENUBET employed a numerical optimization approach relying on a meta-heuristic population-based method like the genetic algorithm also used for the nuSTORM horn optimization [12–14]. The optimization framework developed in [14] for the horn optimization in ENUBET was significantly upgraded for this task since the beamline simulation is much more CPU intensive. The fully optimized beamline has a total length of the transfer line up to the tagger entrance of 26.7 m. The flux at the tunnel entrance for 8.5 GeV/c particles in a 10% momentum bite is 0.4×10^{-3}/pot for K^+ and 4.6×10^{-3}/pot for π^+. The momentum spectra at the tagger entrance obtained with a GEANT4 simulation of the final optimized beamline are shown in Fig. 4. The map of the accumulated ionizing dose in Gy obtained with FLUKA for 10^{20} pot is shown in Fig. 5 (top plot). The dose at the hottest point of the quadrupole closest to the target is < 300 kGy for 10^{20} pot. The maps in the proximity of the target prove that conventional magnets can be operated without risk in a monitored neutrino beam like ENUBET for the entire duration of the data taking.

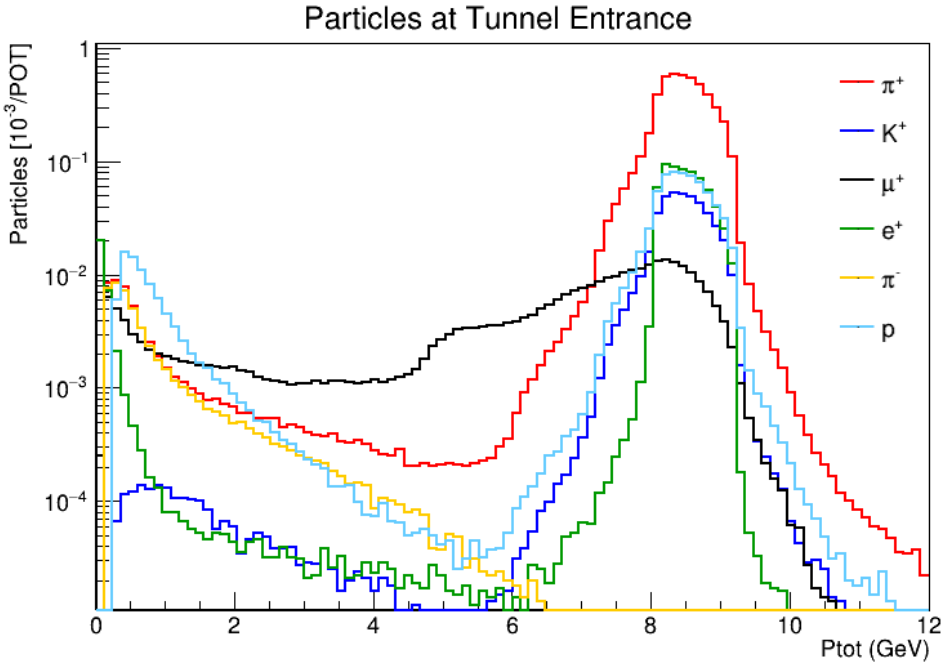

Figure 4: Momentum distribution of particles at the ENUBET tagger entrance as obtained from the GEANT4 simulation after all optimizations.

2.3 Hadron and proton dumps

The final design of the hadron dump at the tagger exit is the result of a dedicated study. It is placed 2 m after the tagger exit and was designed to reduce the background due to backscattering particles reaching the decay tunnel instrumentation. It is composed of a graphite core (50 cm diameter) placed inside a layer of iron (1 m diameter) covered by borated concrete (4 m diameter). Additional borated concrete (1 m thick) is placed in front of the hadron dump leaving an opening for the beam (see Fig. 1). This dump configuration is commonly employed in secondary beamlines to reduce neutron flux. In the last few meters of the tunnel where the neutron fluence is more critical, the ratio between neutrons from the hadron dump hitting the tagger with respect to those one would get with a simpler block of iron is ~ 0.2.

The proton dump has a similar design with three cylindrical layers: a 3 m long graphite core, surrounded by aluminum, which in turn is covered by iron. It is placed at the end of a pipe for the primary 400 GeV proton beam that is filled with air and surrounded by concrete walls (see Fig. 1).

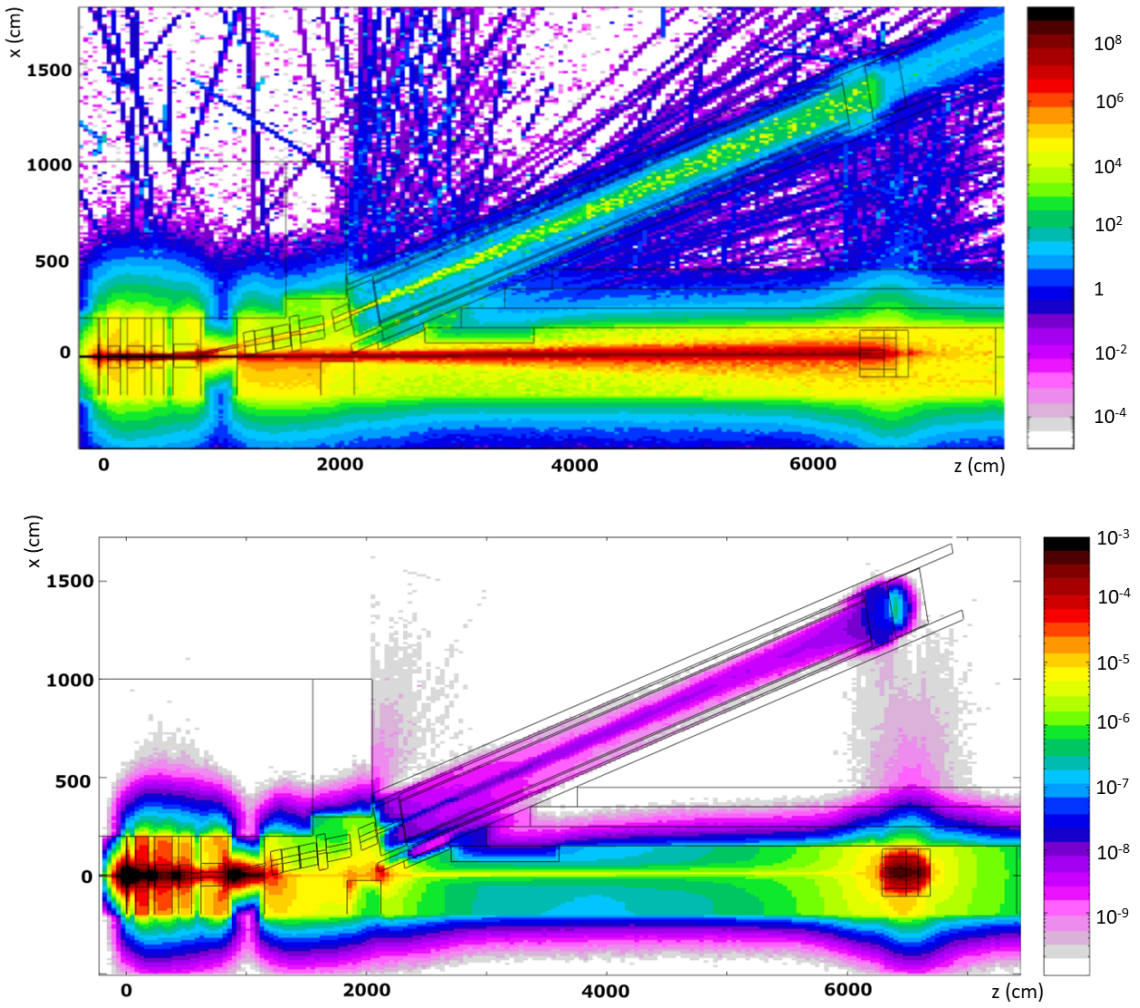

Figure 5: Top: dose map in Gy for 10^{20} pot. The first quadrupole in the map is located between $z \simeq 200$ and 500 cm. Bottom: 1-MeV-eq neutron fluences.

2.4 The instrumented decay tunnel

The simulation of the instrumented decay tunnel is consistent with the design of the ENUBET Demonstrator described in Sec. 3 and is described in detail in [1]. The instrumentation comprises two detectors: a modular sampling calorimeter and a photon veto ("t_0 layer"). Each calorimeter module (Lateral-readout Compact Module - LCM) is made of five slabs of iron interleaved with tiles of plastic scintillators (Eljen EJ-200). The slab and tile cross section is $\sim 3 \times 3$ cm^2 and the thickness is 1.5 and 0.7 cm, respectively. Each LCM thus samples electromagnetic and hadronic showers every 4.3 X_0. Three radial layers of LCMs cover the walls of the tunnel at R=100, 103,

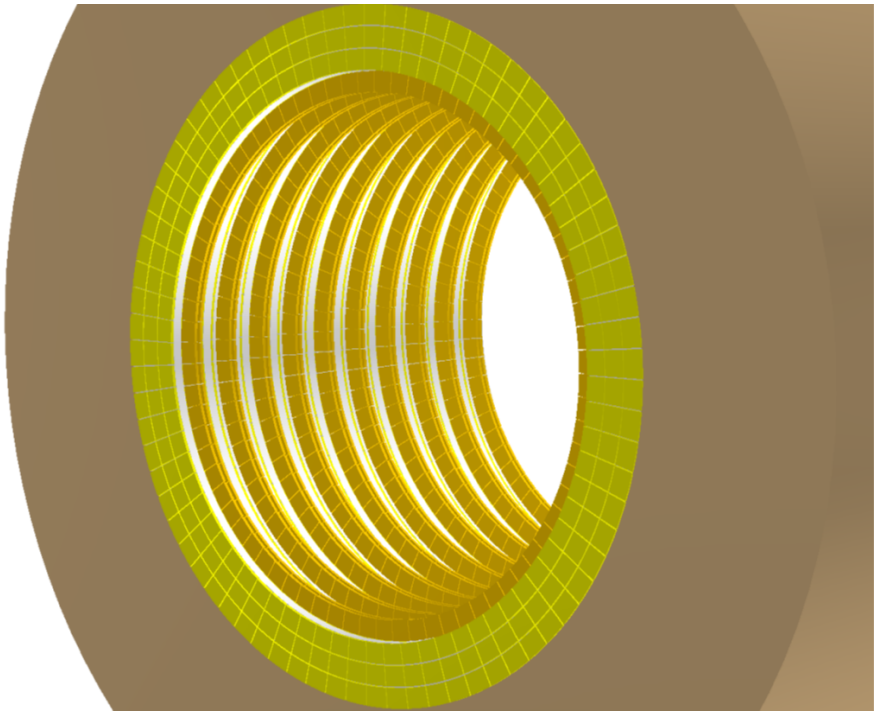

Figure 6: Schematics of the ENUBET instrumented decay tunnel. The three layers of modules of the calorimeter (light green) constitute the inner wall of the tunnel. The rings of the scintillator tiles (doublets) of the photon veto (yellow) are located just below the modules. The optical fibers (not shown) bring the light to the outer part of the tunnel in the radial direction. They cross the neutron shielding (light brown) where the SiPMs (not shown) are positioned.

and 106 cm as in Fig. 6. Each LCM covers an azimuthal angle of 31 mrad and we have 200 LCM per layer at fixed z, where z is the position along the tunnel axis. The dimension of the LCM is a compromise between the need for high-granularity modules for pile-up reduction and particle identification and the total cost of the tunnel instrumentation ($< 10\%$ of the cost of the facility). Even if non-ionizing doses are not critical for the ENUBET beamline, special attention must be paid to neutrons reaching the outer part of the tunnel instrumentation where the SiPMs are located. In the ENUBET Demonstrator and in the beamline simulation, the SiPMs are protected by a shielding layer of Borated polyethylene (BPE, 5% Boron concentration) with a thickness of 30 cm. The neutron reduction induced by adding the BPE layer amounts to a factor of ~ 18, averaging over the expected energy spectrum and it settles at about 7×10^{-11} n/pot/cm^2 in the middle region of the tagger ($7\times$ 10^9 n/cm^2 for 10^{20} pot). Modern SiPMs developed for collider physics can stand $> 10^{12}$ neutrons/cm^2 [15, 16] and these sensors can be employed without risk in the ENUBET instrumented decay tunnel.

The first step for the identification of leptons in the decay tunnel is the event building; we correlate in space and time hits in different LCMs and t_0-layer tiles to select those belonging to the

same particle. Cuts at the event-builder level are optimized to suppress beam halo particles and other mesons' decay modes. Reconstructed events are then processed with a multivariate analysis based on the Multilayer perceptron Neural Network (NN) provided by the TMVA toolkit [17] in order to disentangle the signal from the background. The signal sample for the NN training consists of leptons from kaon decays, while the background sample includes all particles produced by the full GEANT4 simulation of the ENUBET beamline except for signal events. Both samples are produced from a large subsample of particles at the tunnel entrance reconstructed with the same event-building algorithm, resulting in $\sim 10^4$ events for each sample. Two different reconstruction and analysis chains, with specific cuts, NN training samples, and discriminating variables, are used for positrons and muons from kaon decays, respectively. These algorithms are discussed in detail in [1]. The NN gives a positron selection efficiency, including the geometrical one ($\sim$53%), of 21%, and a S/N=2. Thanks to the simpler topology and larger kaon BR, the selection efficiency for muons is even better than positrons. The muon NN shows a signal selection efficiency of ϵ=35.6%, including the geometrical acceptance, and an S/N=5.2.

2.5 Neutrino events at the detector

Considering a neutrino detector with a mass of 500 t, a front face of 6×6 m^2 orthogonal to the neutrino beam, and placed 50 m from the tunnel end, the energy spectra of ν_e and ν_μ interacting through charged-current (CC) within the detector are shown in Figs. 7 and 8, respectively. This detector configuration was inspired by the existing CERN neutrino detectors and, in particular, ProtoDUNE-SP.

The narrow momentum width of the beam ($\mathcal{O}$(5-10%)) can be exploited to provide the neutrino energy on an event-by-event basis, thanks to its correlation with the radial position of the interaction vertex in the neutrino detector. This would be valid for both muon neutrinos from pions and kaons produced by the ENUBET beamline, which can be fully separated in terms of the energy to impact radius dependency. We refer to this method as "narrow band off-axis" (NBOA). The method applies to any two-body decay and it is exploited in ENUBET mostly for ν_μ from pion decays. It relies, however, on the possibility of monitoring the ν_μ flux from pion decay with the same precision as the ν_μ flux from kaon decays. It thus needs an instrumented hadron dump that can monitor forward muons at per-cent level, which is an ongoing part of the NP06 R&D. As shown in Fig. 9, the precision ranges from 10% to 25% in the DUNE energy domain (up to 2 GeV neutrino energy), for which the ENUBET beam is optimized. The worsening of the performance at higher radii and lower energy is due to the neutrino background coming from the beamline, target station, proton dump, and the divergence of the kaon beam. This contribution is heavily suppressed for the higher energy kaon neutrinos, where the performance is significantly better. For this sample, the energy resolution never exceeds 15%.

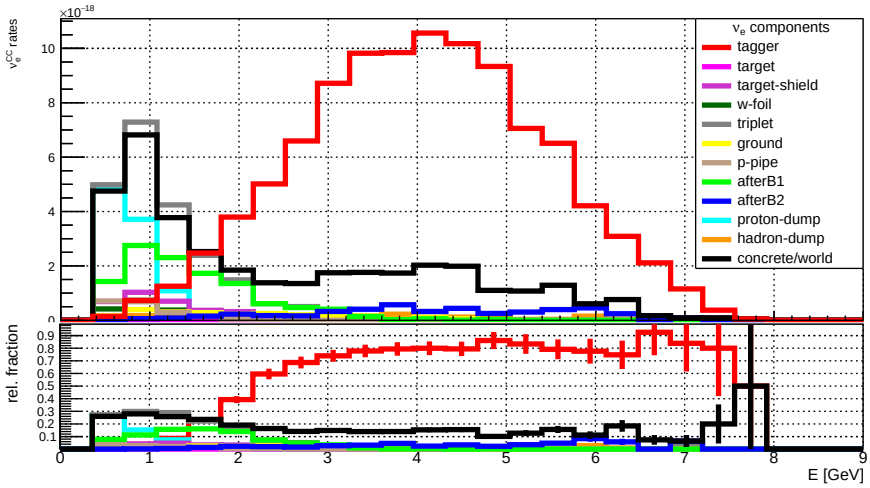

Figure 7: Top: energy spectra of the ν_e interacting in the detector via CC, normalized to 1 pot. We consider a 500 t detector with 6×6 m^2 front face, orthogonal to the neutrino beam, placed 50 m from the decay tunnel end. Each spectrum corresponds to the ν_e^{CC} interactions for which the origin point of the neutrinos is located in a specific region of the ENUBET facility. The red spectrum represents ν_e^{CC} interactions where the neutrinos are produced within the decay tunnel volume (see text for further information). Bottom: fraction of each spectrum relative to the total ν_e^{CC} interactions.

2.6 Assessment of systematic errors

In conventional beams, the knowledge of the neutrino flux at the detector is limited in precision to 5-10%. Uncertainties on the hadroproduction, that is the production of mesons due to the interactions of primary protons in the target material, dominate this systematic value on the neutrino flux. By counting the leptons coming from mesons decays, the ENUBET monitoring technique allows overcoming the hadroproduction uncertainties, thus considerably enhancing the neutrino flux precision. The strategy that we developed to assess the impact of the monitoring technique on the neutrino flux precision is based on the following workflow. A realistic hadroproduction model [18] is fitted to data from NA56/SPY [19] and NA20 [20] experiments that used 450 and 400 GeV/c protons on target, respectively. Thanks to the GEANT4 simulation of the ENUBET facility, mesons outgoing the target, leptons measured in the instrumented tagger, and neutrinos crossing the detector are directly linked, through their evolution histories in the simulation. Therefore, the effect of the hadroproduction uncertainties can be propagated to the lepton observables measured in the calorimeter and to the neutrino flux. The uncertainty propagation is performed by reweighting the Monte Carlo events using the hadroproduction model, where the model parameters are varied taking into account the covariance matrix from the fit to data. For each extraction of the hadroproduction parameters, a new set of MC events is obtained, corresponding to a possible realization

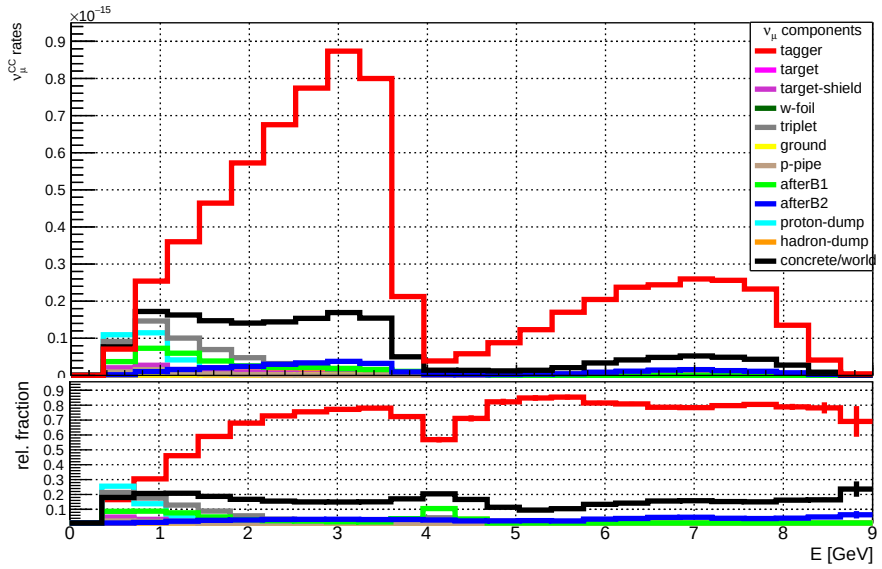

Figure 8: Top: energy spectra of the ν_μ interacting in the detector via CC, normalized to 1 pot. The two populations are related to the neutrinos produced in the two body decay of pions, lower energy spectra ($E_{\nu_\mu} < 4$ GeV), and to the two body decay of kaons, higher energy spectra ($E_{\nu_\mu} > 4$ GeV). We consider a 500-ton detector with 6×6 m^2 front face, orthogonal to the neutrino beam, placed 50 m from the decay tunnel end. Each spectrum corresponds to the ν_μ^{CC} interactions for which the origin point of the neutrinos is located in a specific region of the ENUBET facility. The red spectrum represents ν_μ^{CC} interactions where the neutrinos are produced within the decay tunnel volume (see text for further information). Bottom: fraction of each spectrum relative to the total ν_μ^{CC} interactions.

of the hadroproduction data within their errors. This method is known as multi-universe [21, 22]. From the sets of MC events, the covariance matrices of the lepton observables are computed. Moreover, nominal distributions for lepton observables are built by reweighting the MC events using the hadroproduction model with nominal parameters. A signal plus background model probability density function (PDF) is then assembled by combining the nominal lepton observables and their variations computed from the observables covariance matrices. Pseudo-data are generated out of one of the MC sets, and fitted by building an extended maximum likelihood (EML) from the model PDF. The EML fit is validated through toy-MC experiments generated with the MC sets obtained by applying the multi-universe method. The RooFit package from ROOT is exploited to build the model PDF, perform EML fits, and generate pseudo-data. Given the high correlation between the lepton observables and the produced neutrinos, the EML fit result allows us to set a strong constraint on the flux. The model PDF parametrizes the variation of the lepton observables induced by the hadroproduction and directly constrains the hadroproduction yields through the EML fit. The

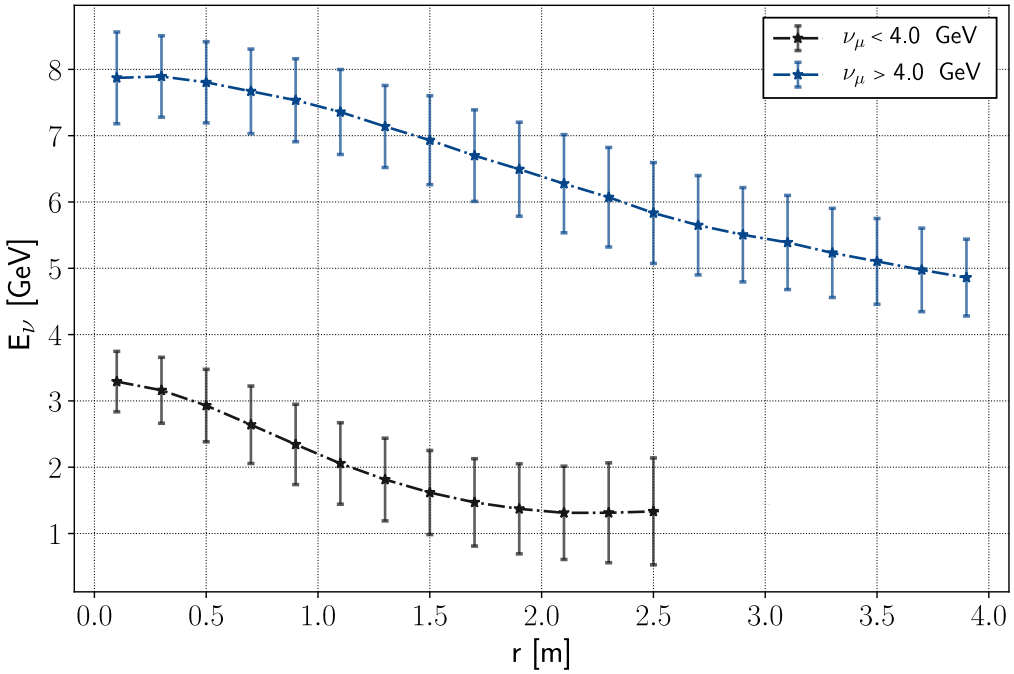

Figure 9: Energy to impact radius dependency for ν_μ CC events for pion (black points laying at $E_\nu < 4$ GeV) and kaon neutrinos (blue points laying at $E_\nu > 4$ GeV). The events are integrated every 20 cm along the detector impact radius dimension: the energy point represents the mean of the distribution, while the error bars its $\pm\sigma$ interval. For the pion neutrino case (low energy) the energy-radius dependency holds up to 2 m radius, with fractional 1σ intervals that go from $\gtrsim 10\%$, to 25% at 2 GeV, and then worsening up to 45% at higher radii and low energy. For the kaon case, it stays within 8 and 15% up to 4 m.

propagation of the residual uncertainties from the constrained hadroproduction model through the multi-universe method allows for computing the neutrino flux covariance matrix after the lepton monitoring is introduced (post-fit result). The result from the described workflow shows that the residual systematic on the neutrino flux due to hadroproduction is of $O(1\%)$, for both ν_e and ν_μ. The same workflow can be extended to determine the impact of the detector effect and beamline subdominant systematics on the neutrino flux. A detailed account of the described procedure, including the results of the assessment of all neutrino flux systematics and the improvement due to the combination of positron and muons will be the topic of a forthcoming publication. The publication is scheduled at the end of 2024.

3 The demonstrator 2023 final layout

The ENUBET demonstrator is the first large-scale prototype of the ENUBET decay tunnel instrumentation. The aim of the detector is assessing the cost-effectiveness and scalability of the chosen technology and ensuring that it can meet the design performances in terms of uniformity, efficiency, particle-identification in a high-flux and irradiation environment. The setup employs a sampling calorimeter for e^+, π^+, μ^+ PID and energy measurement. The calorimeter is coupled to a light tracker (t_0-layer) in the innermost region for e/π^0 separation. The general concept of the tagger region is summarized in Fig. 10.

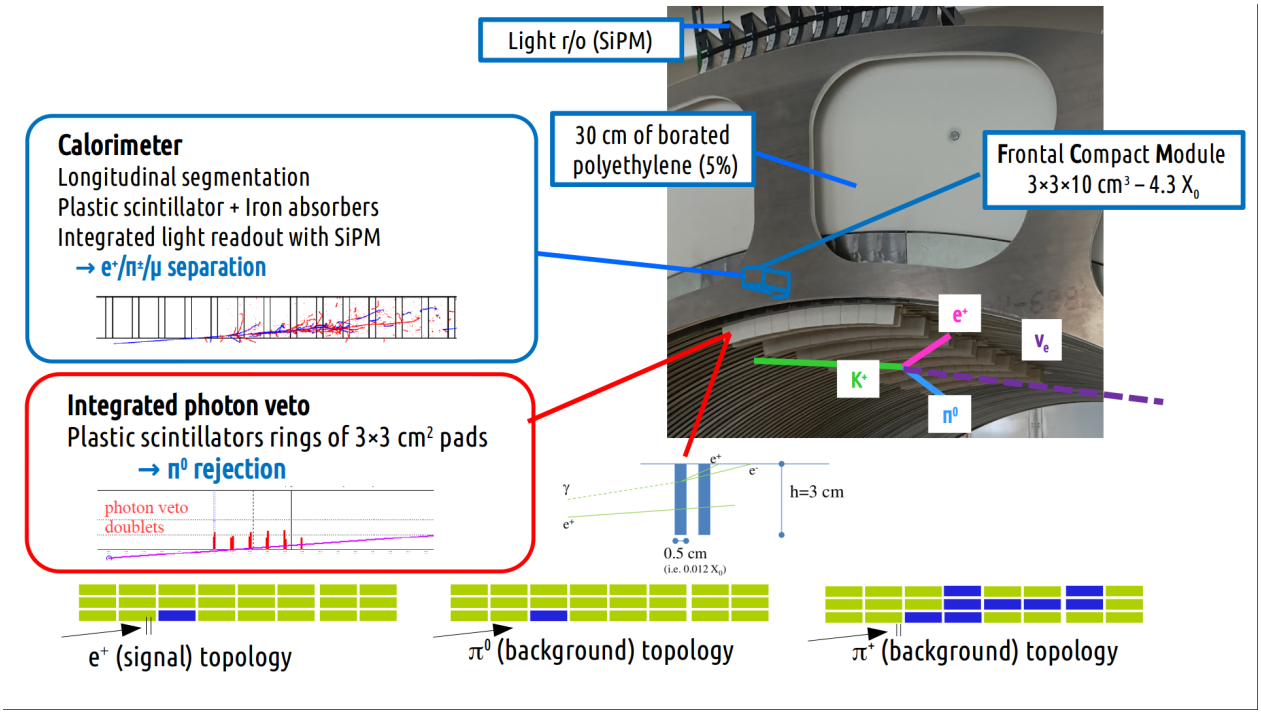

Figure 10: The lepton tagger.

After having been exposed at the CERN-PS T9 area in October 2022, the fraction of instrumented channels of the demonstrator has been significantly extended during 2023 at INFN Legnaro. The 2022 coverage was 10 azimuthal planes and 8 z-planes. To this configuration 25×7 modules were added thus extending the number of channels by more than a factor 3. This is a remarkable milestone of 2023 and it corresponds exactly with what had been planned last year. As each module consists of 5 channels (3 calorimeter cells at different radii and 2 t_0-layer scintillators), the final number of channels amounts to $5 \times (25 \times 7 + 10 \times 8) = 1275$. The pattern of the instrumented portion is shown in Fig. 11 (taken from a GEANT4 simulation of the detector). The demonstrator parameters for the 2022 and 2023 configuration are summarized in Tab. 1.

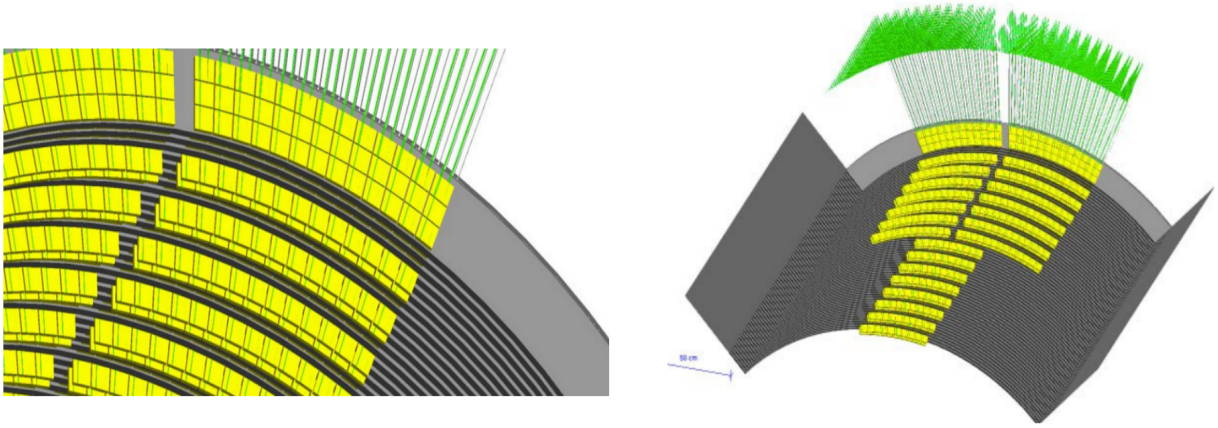

Figure 11: The instrumented fraction from a GEANT4 simulation.

Parameter	2022	2023
Scintillator tiles (7 shapes)	1360	4335
WLS	$\sim$ 1.5 km	$\sim$ 4.5 km
Channels (SiPM)	400	1275
Hamamatsu (50 μm cell)	240 (4×4 mm^2 - calo)+ 160 (3×3 mm^2, t_0)	765+510
Fiber concentrators (FE boards)	80	255
Interface boards	8	22
read-out boards (A5202)	8	22
CAEN digitizers channels	45	0
horizontal movement	$\sim$ 1 m	
vertical tilt	up to $\sim$ 200 mrad	

Table 1: Demonstrator parameters for the 2022 and 2023 test beams.

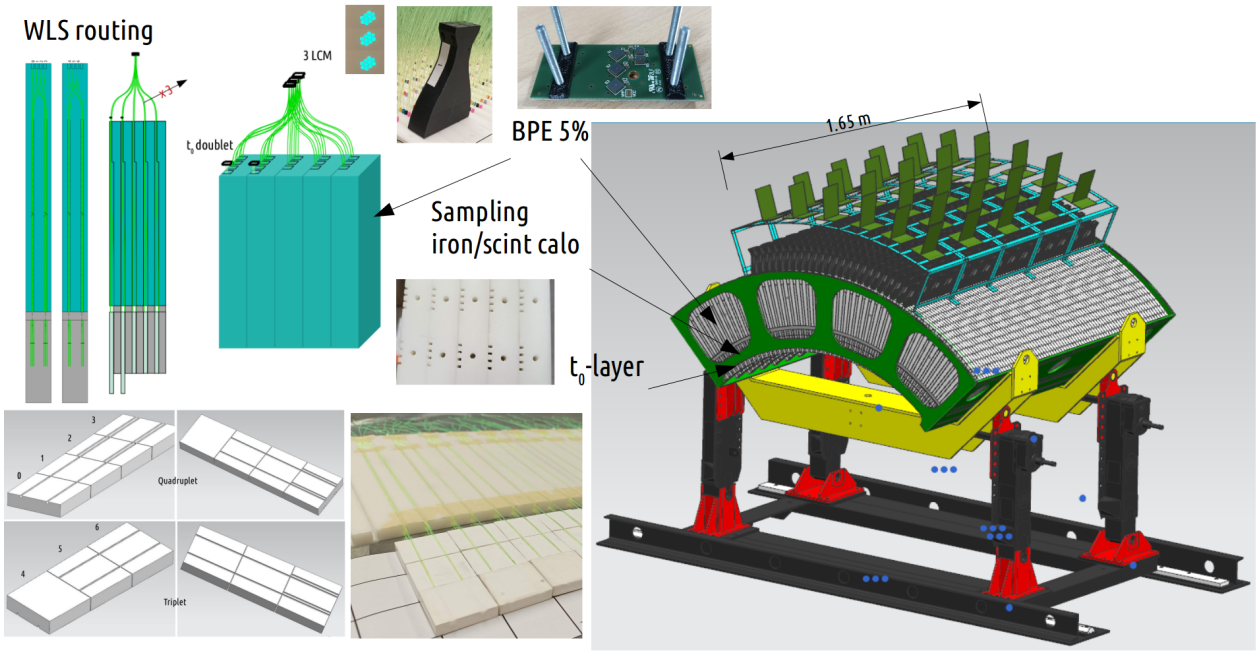

Figure 12: The ENUBET demonstrator.

The detector (Fig. 12) is characterized by a cylindrical symmetry to match with the decay region geometry. It extends for 1.65 m in the longitudinal direction and 90° in azimuth and from 97 to about 150 cm, radially (excluding the electronics). The calorimeter absorbers are 75 zinc-coated iron arcs extending for 15 mm in z, 11 cm radially while scintillators are 7 mm thick and about 3×3 cm^2 in the transverse plane. The structure is extendable to a full 2π coverage. The detector mechanics consists of a crawl sitting on four extensible legs that allow tilting the calorimeter in the vertical plane and adjusting the horizontal position by means of a wheel-rail coupling. The total weight is about 3.5 ton. The mechanics has been proved successful easily allowing to modify the tilt angle by up to 200 mrad and the horizontal position with a range of variation of about 1 m. A 30 cm thick shielding of borated polyethylene slabs with 5% Boron (BPE) protects the photo-sensors from neutron irradiation. Each BPE slab is 22 mm thick and hosts the WLS fibers collecting the light from the scintillators in a sophisticated system of grooves to extract the light from the scintillators (Fig. 12).

3.1 Construction of the 2023 version at INFN-LNL

The structure and assembly of the detector has been covered in the previous annual report and we refer to it for additional information. A visual summary of the steps involved in the detector assembly are reported in Fig. 13. The construction activities were performed at INFN-LNL as in 2022. As anticipated the number of channels has been tripled and the success of this operation has been

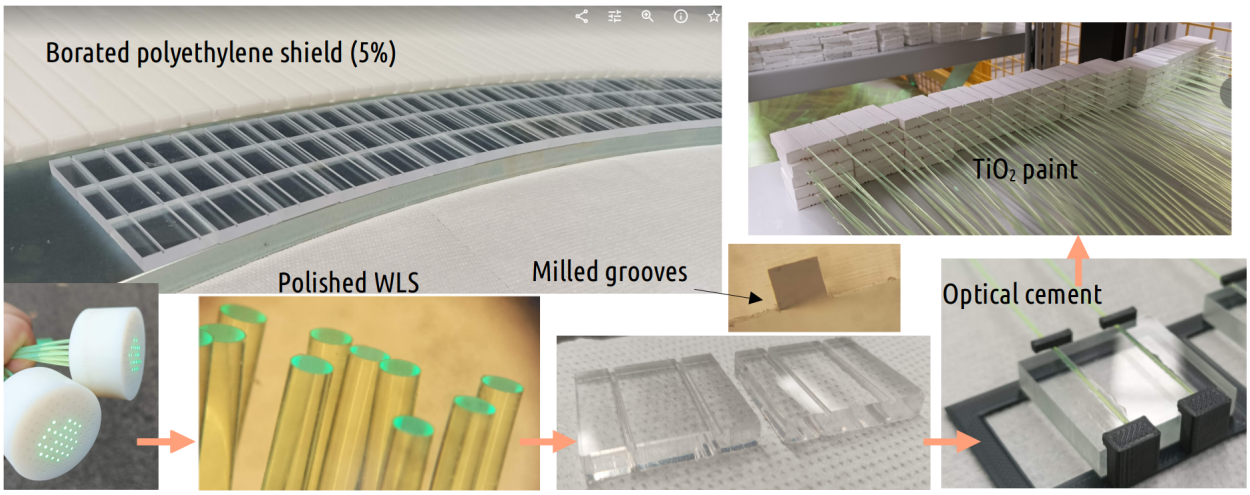

Figure 13: Preparation and pre-assembly phase of the demonstrator. Top left: the iron arc and BPE arcs are visible with scintillators (not yet painted nor glued to WLS). The thickness of the BPE (22.5 mm) is within tolerances equal to the sum of scintillators' (7 mm) and iron thicknesses (15 mm). Grooves on the BPE are needed to host the WLS fibers. Top center: a microscope view of a milled groove. The cross section is squared. Bottom left: WLS fibers inserted into a tool for sandpapering in a plane orthogonal to the fibers' axis. Bottom middle left: the polished WLS fibers seen at the optical microscope. Bottom center right: the scintillators before sandpapering, WLS gluing and painting. Bottom right: WLS gluing with an ad hoc support to keep the WLS fibers horizontal. Top right: a batch of scintillators after WLS gluing and painting with TiO_2, ready for mounting on the iron arcs.

a quite remarkable achievement. The assembly was possible thanks to both local shifters (Padova Univ. and INFN) and from Milano-Bicocca, Bologna, Zagreb (CEMS) and CNRS-Bordeaux (LP2I). The experience obtained in the first phase has helped in optimizing the procedures. This has made possible to successfully cope with such a significant extension of the detector. It should be reminded that the production of the scintillators was initially intended to be done by the UNIPLAST company (Moscow) in collaboration with the INR group using injection molding. The reorganization of the work in a short timescale and the preparation of the detector just based on internal forces was indeed a remarkable achievement obtained by the ENUBET collaboration. Leaving aside some improvements in terms of the organization of the work, the procedures have been substantially unchanged as the demonstrator was already giving good results from the 2022 data taking. Due to technical limitations it was not possible to extend the azimuthal coverage for the 8 z planes that were already instrumented so it was decided to equip the remaining 7 planes with an extended azimuthal coverage of 25 sectors (in place of the initial 10).

3.2 Exposure at CERN in 2023 and highlights of results

The detector was exposed at the CERN-PS T9 area for two weeks in August 2023 and a new exposure is foreseen for late summer 2024. The setup is shown in Fig. 14. We collected data with a mixed pion/muon/proton/electron beam using negative charge and energies from 0.5 to 5 GeV. The electron enriched configuration was also employed. It allowed collecting good samples of electrons at a much higher speed with respect to the previous T9 setup. Last year we have also used a 10 GeV beam to get a sizeable sample of mips (minimum ionizing particles) for calibrations (see later). As usual we employed a pair of silicon trackers to extrapolate the impact point of the particle on the calorimeter with a precision of O(10-100) μm. In 2023 the run acquired in "decay region mode" i.e. pulling the detector out of the beam to measure decay products of kaons was not taken due to lack of time. On the other hand the data taken in this configuration in 2022 have been the subject of a thesis in which it was seen that the achievable statistics in K decays is interesting even though there is still some work to do to disentangle the signal from background due to halo particles. With the acquired information we are going to record more data in this mode in 2024 leveraging on a three-fold larger geometrical acceptance and a better knowledge of the backgrounds. In parallel the characterization of the detector has been extended with a sample of quasi-horizontal cosmic rays that have been collected at INFN-LNL with a suitable trigger composed by a pair of scintillating planes. This has also offered nice material for bachelor students in Padova and Milano.

During the 2023 data taking we have deployed a larger system of CAEN A5202 readout boards (22 in place of 8). Due to problems in the event building among a large number of boards we have acquired the beam separately in the left and right part of the demonstrator and we have not readout part of the channels already tested in 2022. The calorimeter was exposed from the opposite side with respect to 2022 to have a cleaner sample of mips (with less multiple scattering) in the newly instrumented part. In 2024 we are planning to acquire the full detector with a combined DAQ profiting of a new data concentrator board from CAEN that has recently become available.

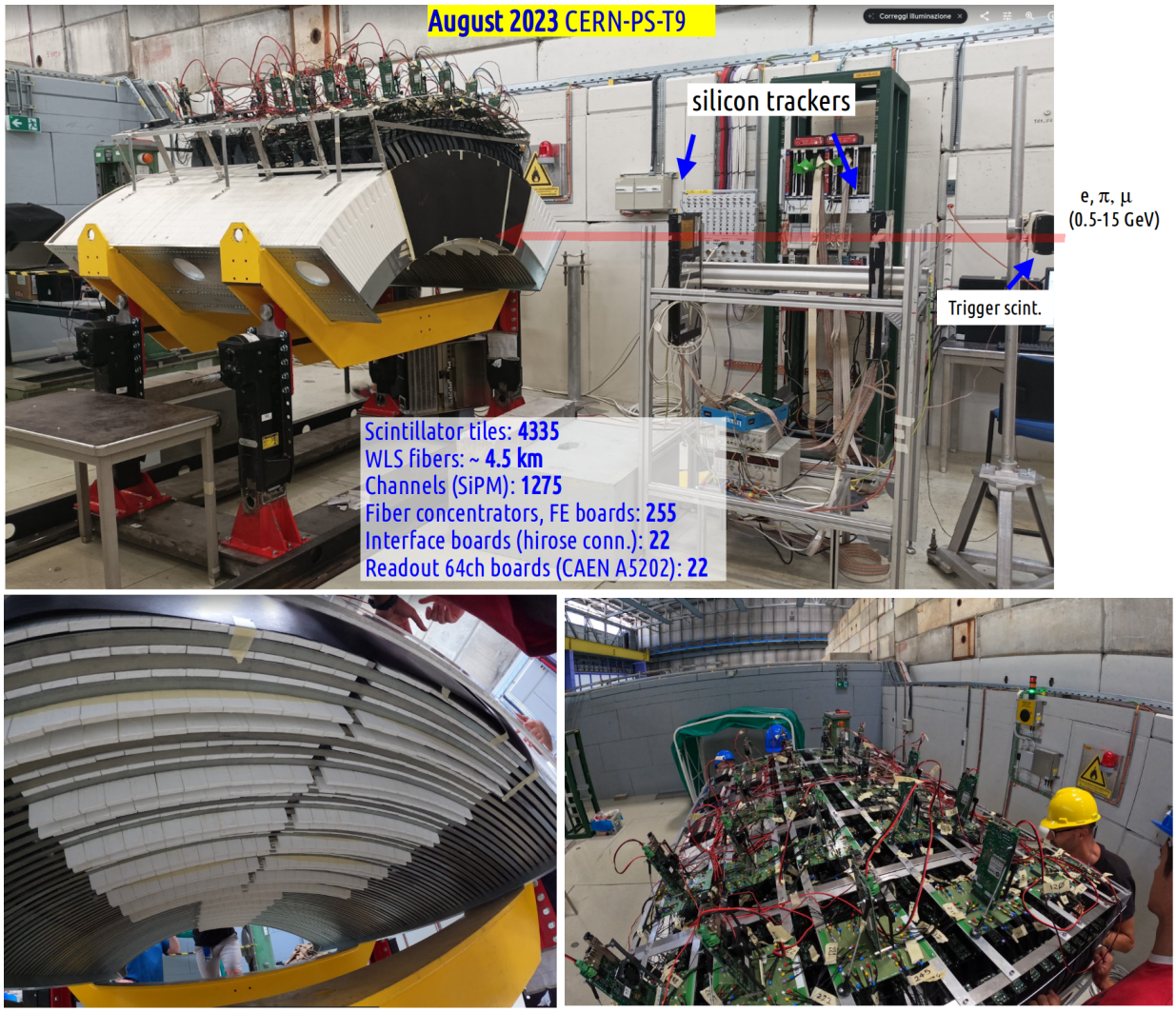

Figure 14: The ENUBET demonstrator at the CERN-PS in August 2023. The detector was hosted into a plastic hut covered with additional thick tissue to ensure light tightness (not shown here).

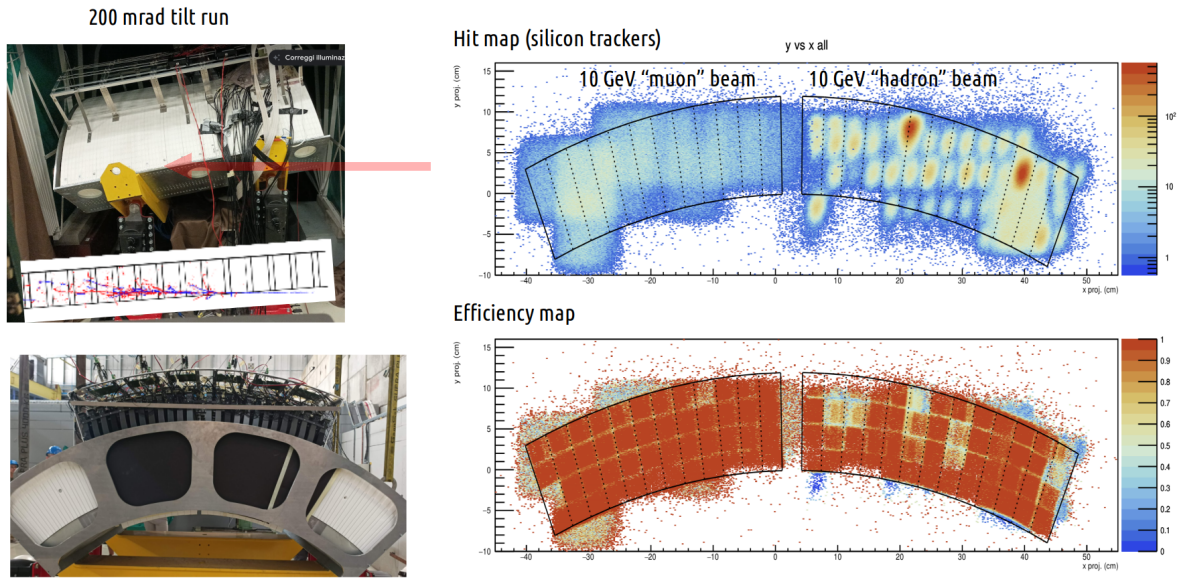

Figure 15: Detector tilting (top left) and calibration runs with mips. (right plots).

3.2.1 Channel equalization

Differences in the response of channels arise from variations in the scintillator thickness (at the 1-2% level for calorimetric modules made of 5 tiles and 2-3% for t_0 channels) and mainly from differences in the WLS-tile and WLS-SiPM optical matching; at second order from the different response of the SiPM. This channel-to-channel non uniformity is corrected for using samples of mips. Due to the large extension of the detector in terms of the beam width (few cm), the calibration procedure is quite time consuming. In 2023 we have used a 10 GeV negative beam with a high content of penetrating pions and muons to equalize the channels of the right part. For the left portion we have used for the first time a quite pure muon beam obtained by using an "electron enriched" target while closing a CuCr1Zr.Electrons have been vetoed using the Cherenkov counters. The beam has been carefully adjusted to "paint" the full front side of the calorimeter. The distribution of the impact points of tracks projected on the front face of the detector can be see in Fig. 15 (top right plot). It can be seen that the left part that has been illuminated with the "muon" beam has a broad beam profile than the right part. The lower plot shows the ratio between the previous distribution and those of tracks associated to at least one energy deposit in the calorimeter above a certain threshold. The pattern of the tiles and some non uniformities clearly appears. This is useful to verify the geometry of the detector and for the definition of solid fiducial regions (i.e. for the electron energy resolution).

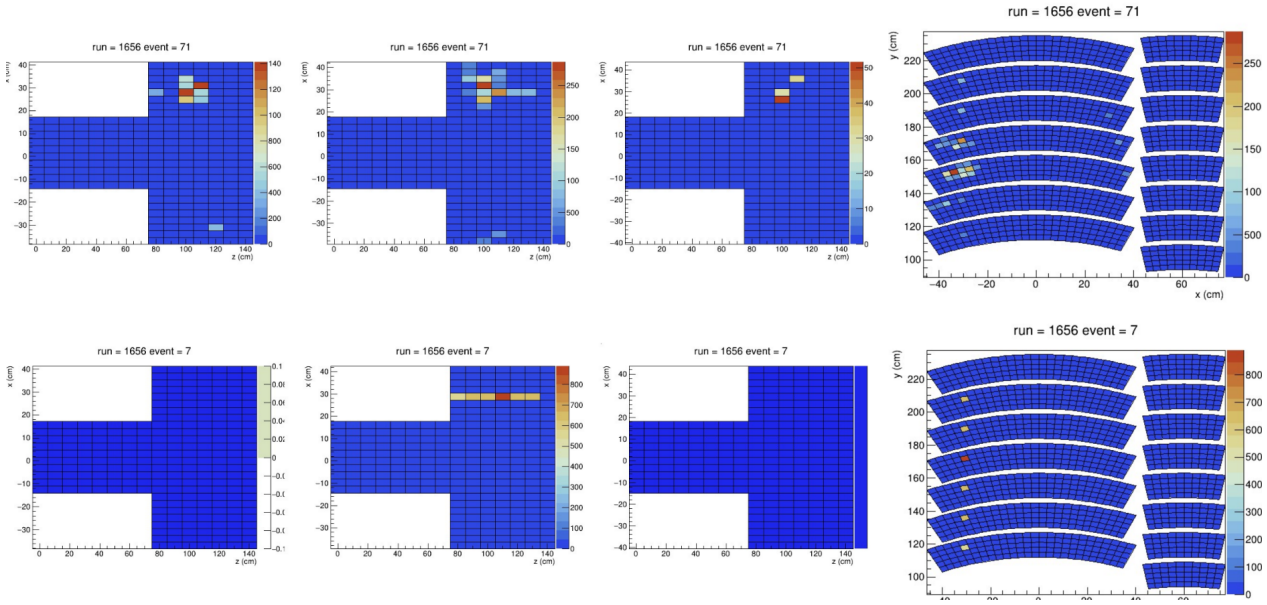

Figure 16: Event displays August 2023. The top row shows an interacting hadron of 10 GeV and the lower one a 10 GeV muon candidate. The plots in the first three rows from the left are a $z - \phi$ view in three radial layers while the last column is a $r - \phi$ view for the 15 different z layers (the ϕ coverage, as explained, depends on z).

3.2.2 GEANT4 simulation

The new version of the detector has been modeled using GEANT4 (Fig. 11). The simulation includes the precise description of the angular and spatial distributions of the beam as measured by Silicon tracking chambers, the calibration procedure with mips and the non-uniformity of light collection; a model to describe photo-electron Poisson fluctuations and a toy model for the cross-talk between channels. The optical simulation can be switched on but it has so far not yet been exploited. A subtle but substantial improvement has been the description of the dead regions between tiles that turns out to have a significant beneficial impact to improve the data/Monte Carlo agreement for the energy resolution. The software for data quality monitoring and channel mapping has also been substantially improved. As an example the event displays of two recorded events are shown in Fig. 16. The top one correspond to an interacting hadron of 10 GeV while the second is a muon candidate.

3.2.3 Electron energy resolution

In order to measure the energy resolution for electrons, dedicated runs at 0.5, 1, 2, 3, 4, and 5 GeV/c were taken. The total visible energy deposit for each event was estimated by adding together the equalized signals of all LCMs. Čerenkov detectors were used to select only electron tracks. To ensure

good containment of the electromagnetic shower, only electrons with a primary track (projected to the front face of the calorimeter) impinging at least 2 Molière radii ($R_M \simeq 1.72$ cm in iron) from the edges of the calorimeter were considered. The energy deposit spectra (Fig. 17, top) were fitted with a Gaussian function. Resolution as a function of beam energy is shown in Fig. 17, bottom) and parametrised with $\frac{\sigma_E}{E} = \frac{a}{\sqrt{E}} \oplus \frac{b}{E} \oplus c$. The data/MC agreement is about correct. We are finalizing the study of the impact of systematics (photo-electron statistics, impact of dead regions, cross talk).

3.2.4 Study of cross-talk

Cross-talk can arise from direct light leakage between adjacent tiles in case the painting layer might be damaged or too thin[2]. In addition it can arise if WLS fibers collect light from a different tile with respect to the one they are glued. This can happen again, if the painting is not completely light tight, because the fibers carrying light from tiles at low r pass near the tiles at higher-r through the so-called "transit grooves". The occurrence of light escaping the WLS and reentering the scintillator is considered negligible from first principles. For this study it was mandatory to select pure muon samples as pions interactions can easily mimic a cross-talk effect. After selecting a muon crossing the middle of a certain tile, the signals in the other tiles were studied. In general the signals are almost always compatible with the background and the effect if present is at the % level.

With 2023 data we have gained a much better insight into this effect thanks to better samples of mips. A systematic study was done for the most upstream z layer. In this study, for each LCM a sub-set of events was selected such that:

- the primary track falls within a 1.5×1.5 cm^2 fiducial cut, centered on the LCM;
- the signal registered in the LCM is higher than 0.75 mips;
- the total signal in the first layer is compatible with that of a muon, so the deposited energy is ~ 1 mip. This is done in order to ensure that the particle - be it a muon or, for example, a pion - has not (yet) started an electromagnetic shower in this z layer.

We define for all channels of the upstream z layer, which are identified by their (R, ϕ) coordinates:

$$\chi(R, \phi) = \frac{PH_{eq}(R, \phi)}{PH_{eq}(R_0, \phi_0)}$$

Where $PH_{eq}(R_0, \phi_0)$ is the equalized signal registered by the LCM currently being considered. The $\chi(R, \phi)$ was then plotted for all channels in the upstream z layer. An example of the resulting plot is shown in Fig.18. While some cross-talk seems to be indeed present, as some channels seem to have non-negligible values for $\chi(R, \phi)$, such values are always of a few %. In order to better understand the potential effects of such cross-talk, a similar effect was implemented on the simulation. The effect on the resolution is small. We are consolidating the analysis by studying the dependence of

[2]We used two applications of the paint.

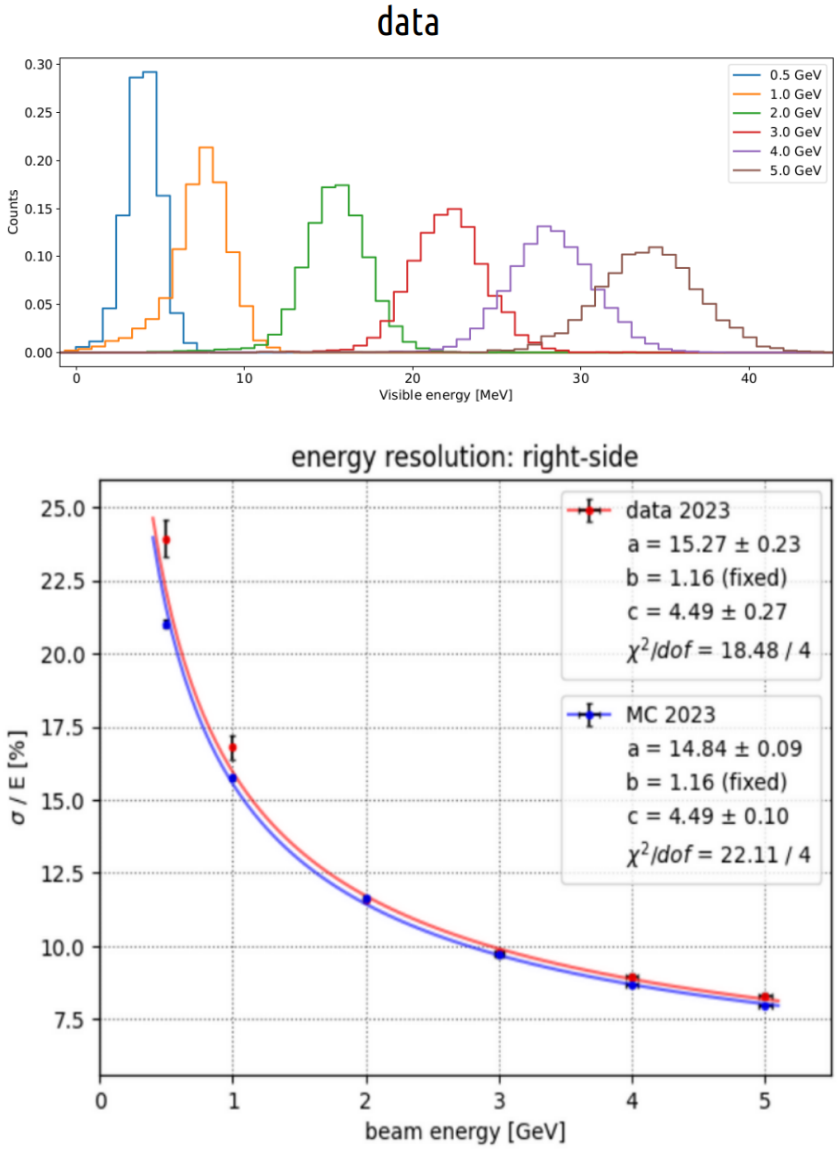

Figure 17: Energy resolution results. Top: equalized visible energy observed in the fiducial volume in data for different beam energies. Bottom: energy resolution vs E_{beam} in data (red) and Monte Carlo (blue).

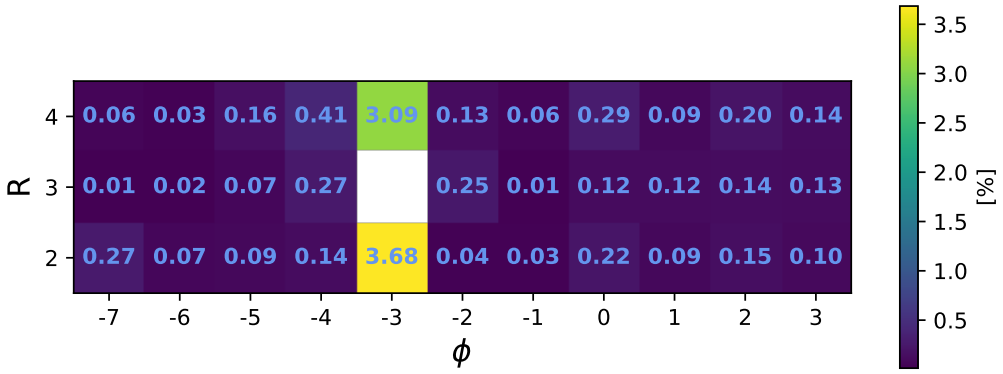

Figure 18: Cross-talk values computed for the left side of the Demonstrator, with LCM $(R_0, \phi_0) = (3, -3)$ chosen as reference.

the cross-talk estimator for the four neighbouring cells on the position of the cell (not shown). We will also simulate the procedure with the Monte Carlo to rule out possible artifacts due to energy leakage.

The analyses are going to be completed in the next months in view of a publication. The most important remaining points to address are the presence in the equalization coefficients of two populations (we are making some tests in the reproducibility of the optical coupling between the SiPM and the WLS fibers bundles with cosmic rays). Another direct measurement which is being finalized isthe average number of photoelectrons for a mip deposit. We would like to obtain this number with an independent electronics (based on digitizers readout of highly amplified signals) and check it with the assumption in the simulation and the estimates obrained with the CAEN electronics. We will also finalize the analysis of inclined runs and make some test of data-Monte Carlo consistency for particle discriminating variables. An initial work in this direction is shown in Fig. 19 where three discriminating variables (see caption) are used to separate electrons from a mixture of muons and hadrons at 3 GeV.

In the future test beam we will exploit a new DAQ capable of reading out the full detector (with the CAEN "data-concentrator" based on optical fiber synchronization), we will test for some channels a new low-cost digitizer developed at INFN-PD in the context of the CTA+ experiment. Finally we will try to replace the darkening "garage" with a more compact customized light tight box made with black polycarbonate that is in construction.

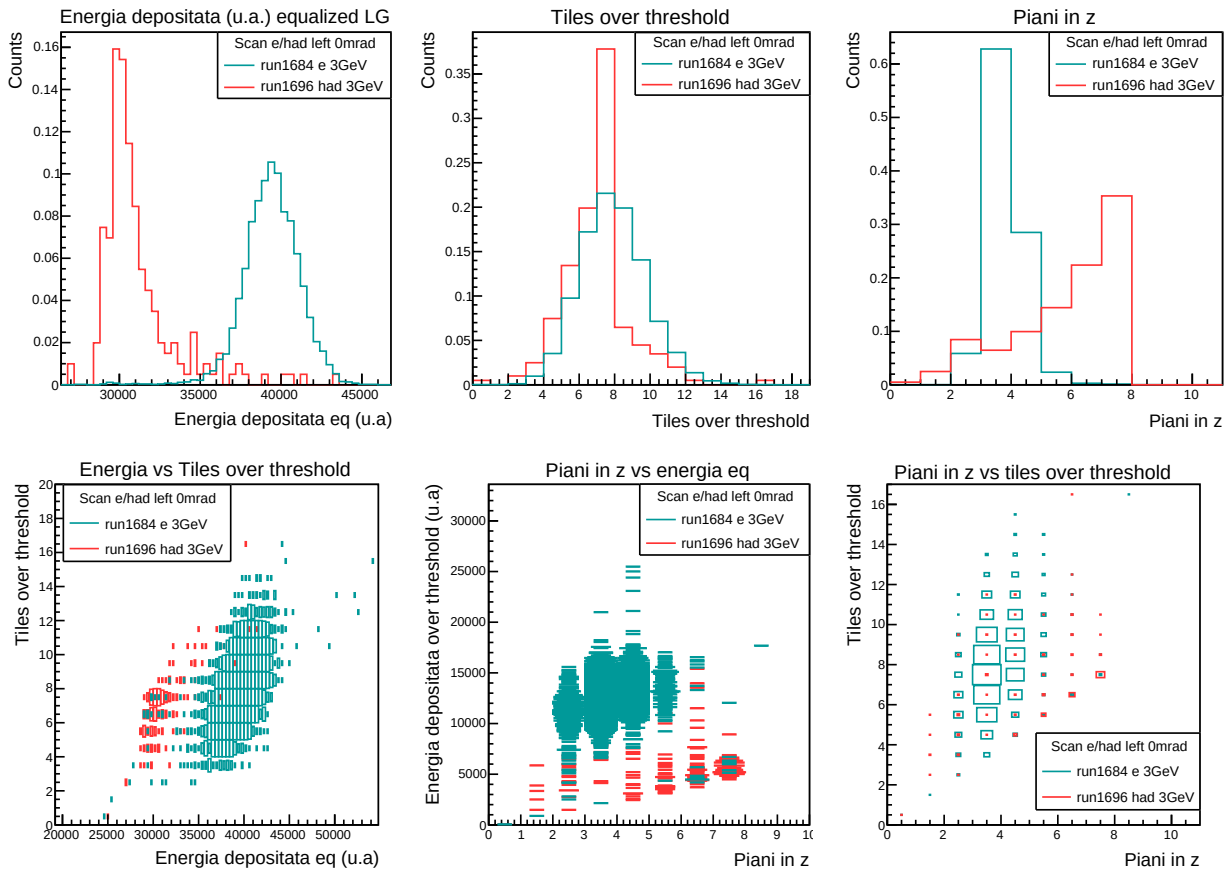

Figure 19: Electron (green) and "hadron" (red) runs at 3 GeV. In the top row, from left to right we have the total deposited energy, the number of channels above a threshold and the number of z planes with at least one channel above threshold. In the bottom row we show the correlations of these three estimators.

4 SBN@PBC

The previously mentioned ENUBET beamline has a couple of disadvantages. First, it is designed to focus on the area of interest for DUNE, but it does not provide enough data in the 1 GeV range that is important for HyperKamiokande. Additionally, it requires a large number of protons on target, which creates issues for the CERN fixed target program, especially now that SHiP has been approved. In order to address these drawbacks, CERN is taking action under the Physics Beyond Collider initiative. They have brought together CERN accelerator specialists (led by N. Charitonidis), the NuTAG Collaboration (headed by M. Perrin-Terrin), experts from DUNE and HyperKamiokande, as well as the developers of ProtoDUNE. The SBN@PBC beamline is inspired by the ENUBET multi-momentum beamline developed by N. Charitonidis and E. Parozzi from BE-EA-LE in 2021-2023 [9].

The multi-momentum beamline is based on [1] but allows for runs at different secondary momenta (4, 6, and 8.5 GeV/c). This way, ENUBET at CERN can enrich the statistics in the 1 GeV region and improve the cross-section measurement of relevance for Hyper-Kamiokande. It is based on existing CERN magnets and was optimized using TRANSPORT, MAD-X, FLUKA, and G4beamline. This beamline is described in the 2023 ENUBET Annual Report. In the course of 2023, the beamline was re-optimized using a multi-objective genetic algorithm (MOGA) employing BDSIM instead of G4Beamline. The optimization process of the beamline is rather extensive, and takes into account the target (16 targets analyzed), the length of 7 drift spaces, 18 quadrupole parameters (6 magnets with different length, aperture, gradient) for a total of 26 free parameters. The MOGA is operated in multiple objective mode: it maximises kaon and pion transmission and requires the beam size to be as small as possible in the momentum selection and the decay tunnel (3 objectives). Preliminary results were presented by M. Jebramcik at the PBC Annual Meeting on March 26, 2024 [23]. The current design reduces the pot needs by a factor of 3 compared with the ENUBET beamline and points toward both NP04/ProtoDUNE-SP (now called ProtoDUNE-HD) and NP02/ProtoDUNE-DP (ProtoDUNE-VD). The use of both detectors, possibly complemented by a smaller water Cherenkov detector (WCTE [2]) further reduces the pot requirements. Noteworthy changes as a consequence of the optimization process are:

- The optimized beamline is 7 m shorter
- Quadrupoles got shorter and the aperture gradient was re-optimized
- The beam remains much smaller throughout the decay tunnel than the multi-momentum beamline envelope
- The graphite target was changed from $L = 0.7$ m, $r = 3$ cm to a CNGS-like target ($L = 1.3$ m, $r = 3$ mm)

As a result, the overlap of the acceptance with the target yield is much improved after the optimization process as shown in Fig. 20. The yield of kaons (pions) shows a significant increase, reaching 14.1×10^{-4} K/pot (2.15×10^{-2} π/pot), which is a remarkable improvement compared to

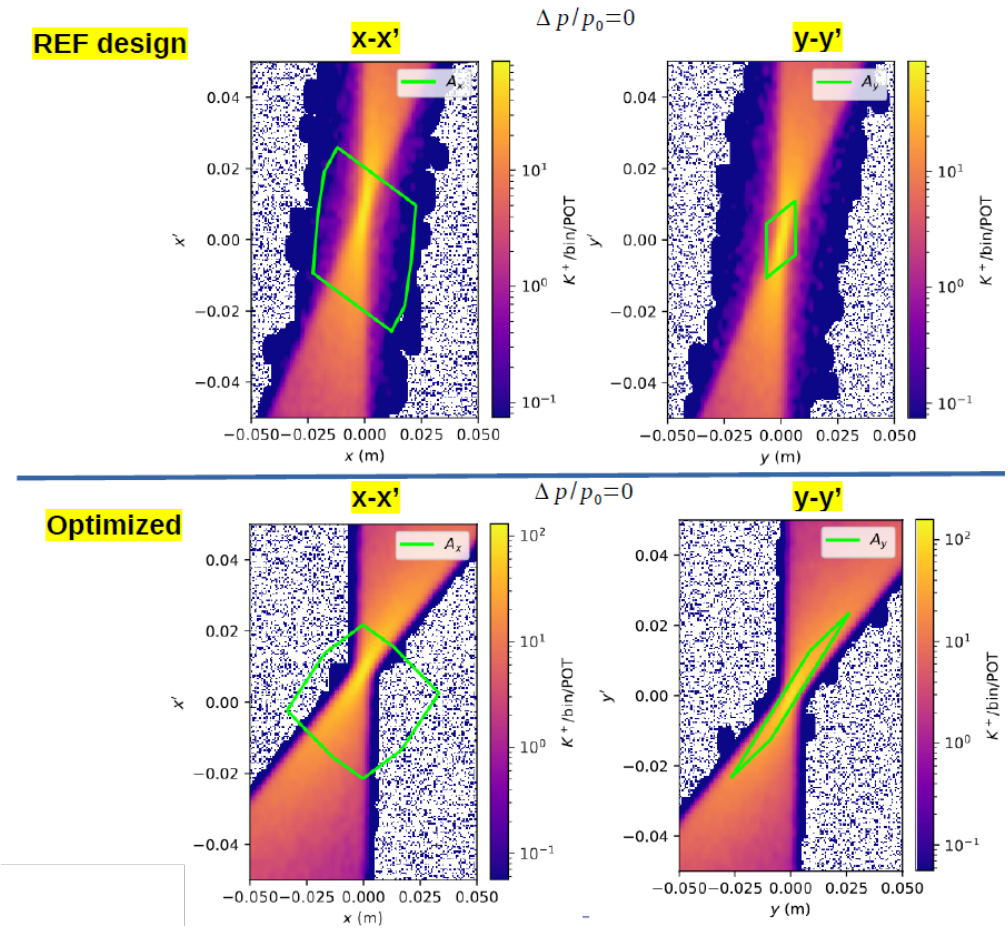

Figure 20: Beamline acceptance before (top plot) and after (bottom plot) the optimization. Further information is available in [23].

the findings in [1]. Furthermore, it is now possible to track mesons within the transfer line using fast silicon trackers that employ the same technology currently being developed for LHC-HL. This new capability allows for the collection of a subset of neutrino events that are not only monitored but also *fully tagged* [1, 4]. A tagged neutrino beam utilizes detectors with a time resolution of less than 100 ps to connect the observed neutrino interaction in the detector with the corresponding lepton in the decay tunnel and to its parent meson. This connection greatly enhances the energy resolution of the neutrino, reducing it from 10-15% to just a few percent, surpassing the capabilities of ENUBET.

To achieve the ENUBET physics goals with the two ProtoDUNEs, SBN@PBC requires 1×10^{19} pot. The PBC ECN3 Beam Delivery Task Force has performed the analysis of pot-per-year for TCC2 while featuring dedicated cycles for SHiP (ECN3), and implementation scenarios for SBN@PBC in

this concrete framework are discussed in [23].

5 Conclusions and remaining tasks

The NP06 programme is now close to completion. The remaining tasks will be addressed in 2024-2025 and are summarized in the following.

- The systematic reduction programme aims at reaching a flux uncertainty below 1%. To provide this demonstration we need to consider also subdominant systematics other than hadroproduction uncertainties. They are the uncertainties in detector response (calibration and aging), magnet currents, and uncertainties in the beamline material budget. The work is well underway and we aim to a publication by the end of 2024. This study also allows us to explore the possibility of instrumenting only a portion of the decay tunnel instead of the entire 40 meters. This approach would imply further cost savings.

- The NBOA method also relies on observing muons produced by pion decays in the forward region of the decay tunnel. The development of the instrumented hadron dump is being carried out as part of the PIMENT project (Picosecond MicroMegas for ENUBET [24]), which is funded by the French ANR for the years 2022-2024. A prototype will be tested at T9 (ENUBET) and in the North Area (RD51) in 2024. The SPSC has specifically reserved a two-week period in T9 for ENUBET in the summer of 2024, although the exact dates are still being discussed. We have requested the SPS coordinator to move this period to September in order to avoid any conflicts with the RD51 tests. The optimization of the hadron dump for monitoring muons produced by pion decays is a joint task for both ENUBET at CERN and ESSνSB+ [3]. Therefore, in February 2023, we established a collaborative group (Athens, CNRS, INFN, Thessaloniki, Zagreb) to tackle this challenge, even after the completion of PIMENT.

- During the upcoming ENUBET beamtime, we will utilize an improved DAQ system to read the Demonstrator. This advancement enables us to simultaneously read all LCMs, unlike in 2023 when we could only read 50% of the channels at a time. Additionally, in 2024, we plan to experiment with a new digitizer that is being developed for the CTA+ telescopes. This digitizer meets the cost and scaling criteria for both ENUBET and SBN@PBC. To conduct this test, we will use a subset of channels from the Demonstrator.

Given the remarkable success of the NP06 R&D, the potential implementation of this technique at CERN is being investigated by PBC, as discussed in Sec. 4. This activity is also motivated by the anticipation of the European Strategy. We aim at a White Paper for a new generation of high-precision cross-section experiments to be submitted to the Strategy in 2025. To achieve this

[3]This EU-funded project has a Working Package (WP6) that is investigating the potential use of the ENUBET technique at the European Spallation Source [25].

objective, the ENUBET collaboration has intensified its endeavors to assess the physics capabilities of the ProtoDUNEs for cross-section measurements, with the intention of publishing a dedicated paper in 2025.

References

[1] F. Acerbi et al., Eur. Phys. J. C **83**(10), 964 (2023). DOI 10.1140/epjc/s10052-023-12116-3

[2] L. Botao, T. Dieminger, M. Franks, A. Gendotti, et al., The Hyper-K Underwater Electronics Assembly project. Tech. rep., CERN, Geneva (2023). URL `https://cds.cern.ch/record/2867639`

[3] S. V. Garode, S. S. Chinchanikar, C. S. Garde, A. R. Mache, S. G. Joshi, N. Deshmukh, P. Patil, A. Konaka, and M. Hartz, J. Phys. Conf. Ser. **2374**(1), 012035 (2022). DOI 10.1088/1742-6596/2374/1/012035

[4] A. Baratto-Roldán, M. Perrin-Terrin, E. G. Parozzi, M. A. Jebramcik, and N. Charitonidis, (2024). arXiv:401.17068

[5] G. Battistoni, T. Boehlen, F. Cerutti, P. W. Chin, L. S. Esposito, A. Fassò, et al., Annals of Nuclear Energy **82**, 10 (2015)

[6] T. Böhlen, F. Cerutti, M. Chin, A. Fassò, A. Ferrari, P. G. Ortega, A. Mairani, P. R. Sala, G. Smirnov, and V. Vlachoudis, Nuclear data sheets **120**, 211 (2014)

[7] T. J. Roberts, K. Beard, S. Ahmed, D. Huang, and D. M. Kaplan, in *Proc. PAC*, vol. 2013 (2011), vol. 2013, pp. 373–375

[8] R. P. Feynman, Phys. Rev. Lett. **23**, 1415 (1969). DOI 10.1103/PhysRevLett.23.1415

[9] E. G. Parozzi. Design and optimisation of a variable momentum secondary beamline for the NP06/ENUBET project (2022). Ph.D. Thesis, Univ. of Milano Bicocca

[10] T. J. Roberts and D. M. Kaplan, Conf. Proc. C **070625**, 3468 (2007). DOI 10.1109/PAC.2007.4440461

[11] M. Cauchi, R. Assmann, A. Bertarelli, F. Carra, F. Cerutti, L. Lari, P. Mollicone, S. Redaelli, and N. Sammut, Physical Review Special Topics - Accelerators and Beams **18** (2015). DOI 10.1103/PhysRevSTAB.18.041002

[12] M. J. Kochenderfer and T. A. Wheeler, *Algorithms for Optimization* (MIT press, 2019)

[13] A. Liu, A. Bross, and D. Neuffer, Nucl. Instrum. Meth. A **794**, 200 (2015). DOI 10.1016/j.nima.2015.05.035

[14] M. Pari, Study and development of SPS slow extraction schemes and focusing of secondary particles for the ENUBET monitored neutrino beam. Ph.D. thesis, Universitá degli Studi Di Padova, Dipartimento di Fisica e Astronomia G. Galilei, Padova (2021). URL https://hdl.handle.net/11577/3426254

[15] Y. Musienko, A. Heering, R. Ruchti, M. Wayne, Y. Andreev, A. Karneyeu, and V. Postoev, JINST **12**(07), C07030 (2017). DOI 10.1088/1748-0221/12/07/C07030

[16] E. Garutti and Y. Musienko, Nucl. Instrum. Meth. A **926**, 69 (2019). DOI 10.1016/j.nima.2018.10.191

[17] A. Hocker et al. TMVA - Toolkit for Multivariate Data Analysis (2007). arXiv:physics/0703039

[18] M. Bonesini, A. Marchionni, F. Pietropaolo, and T. T. de Fatis, Eur. Phys. J. C **20**(1), 13 (2001)

[19] G. Ambrosini, R. Arsenescu, K. Bernier, C. Biino, M. Bonesini, et al., Eur. Phys. J. C **10**(4), 605 (1999). DOI 10.1007/s100520050601. URL https://doi.org/10.1007/s100520050601

[20] H. W. Atherton, C. Bovet, N. Doble, G. von Holtey, L. Piemontese, A. Placci, M. Placidi, D. E. Plane, M. Reinharz, and E. Rossa, (1980). DOI 10.5170/CERN-1980-007

[21] M. Kordowsky. Error bands from the many universes method. Minerva note, n.7433

[22] B. Messerly et al., EPJ Web Conf. **251**, 03046 (2021). DOI 10.1051/epjconf/202125103046

[23] Physics beyond collider annual workshop. https://indico.cern.ch/event/1369776/. Talk by M. Jebramcik. Workshop held at CERN, March 25-27, 2024

[24] T. Papaevangelou. Développement d'un détecteur PICOSEC-micromegas pour ENUBET – PIMENT (2022). Available at https://anr.fr/Projet-ANR-21-CE31-0027

[25] First annual meeting of the essnusb+ project. https://indico.cern.ch/event/1309436/. Workshop held at CERN, October 16-20, 2023